

Received 2 June 2024; revised 21 June 2024; accepted 26 June 2024. Date of publication 2 July 2024; date of current version 5 September 2024.  
 The review of this article was arranged by Editor Z. Zhang.

Digital Object Identifier 10.1109/JEDS.2024.3422292

# Directly Fabricated Flexible Photodetector Based on TiO<sub>2</sub>-Doped Carbon Nanosheets Film

YUNLONG ZHANG<sup>ID 1</sup>, XIAOLIN LI<sup>1</sup>, ZHIPENG CAO<sup>2</sup>, QIANG WU<sup>3</sup>, GONG CHEN<sup>ID 4</sup>,  
 BO WEN<sup>1,3</sup>, DONGFENG DIAO<sup>1</sup>, AND XI ZHANG<sup>ID 1,4</sup>

<sup>1</sup> School of Mechatronics and Control Engineering, Guangdong Provincial Key Laboratory of Micro/Nano Optomechatronics Engineering, Shenzhen University, Shenzhen 518060, China

<sup>2</sup> R&D Department, Shenzhen Lihuy Medical Technology Company Ltd., Shenzhen 518060, China

<sup>3</sup> Research Center of Medical Plasma Technology, Shenzhen University, Shenzhen 518060, China

<sup>4</sup> R&D Department, Shenzhen Milebot Robotics Company Ltd., Shenzhen 518060, China

CORRESPONDING AUTHOR: X. ZHANG (e-mail address: zh0005xi@szu.edu.cn)

This work was supported in part by the National Natural Science Foundation of China under Grant 52275563 and Grant 62104155; in part by the NSF of Guangdong Province under Grant 2022A1515011667; in part by the Shenzhen Foundation Research Key Project under Grant JCYJ20200109114244249; in part by the Shenzhen Excellent Science and Technology Talent Training Project under Grant RCYX20231211090249068; and in part by the Youth Talent Fund of Guangdong Province under Grant 2023A1515030292.

(*Yunlong Zhang and Xiaolin Li contributed equally to this work.*)

This article has supplementary downloadable material available at <https://doi.org/10.1109/JEDS.2024.3422292>, provided by the authors.

**ABSTRACT** Flexible photodetector is crucial for the intelligent industrial applications. However, the optical-sensitive materials are usually grown in a high temperature and then transferred onto the flexible substrate. This paper reported a directly fabricated flexible photodetector based on TiO<sub>2</sub>-doped Graphene Nanosheets Embedded Carbon (GNEC) film. An Electron Cyclotron Resonance (ECR) system was employed to in-situ deposit TiO<sub>2</sub>-doped GNEC film on a polyimide substrate, which were subsequently sensitized with N719 dye to fabricate the TiO<sub>2</sub>@GNEC photodetector. The GNEC film contains vertically aligned Graphene Nanosheets (GNs), which exhibit high-density edge states. The edge states suppress the recombination rate of photo-generated electron-hole pairs, thereby significantly enhancing the photo-responsive performance. The photodetector demonstrates a high photo responsivity of 0.82 mA/W and a response time of 1.93 seconds. Due to the in-situ manufacturing capabilities of the ECR system, which avoids defects from secondary material transfers, the photodetector array exhibits excellent consistency and achieves clear recognition of light patterns in both flat and bent states.

**INDEX TERMS** Photodetector, nanomaterials, cyclotron resonance, vertical graphene.

## I. INTRODUCTION

Photodetectors are widely used in biochemical assays and industrial production, with flexible and array-based photodetectors becoming a hot research topic in recent years [1], [2], [3]. In the fabrication process of flexible photodetectors, the photosensitive materials are usually grown at high temperature on a rigid substrate, and then transferred to a flexible substrate [4]. Developing a method for integrated fabrication of flexible photodetectors at low temperatures is a key requirement in this field [5], [6]. TiO<sub>2</sub>, as a crucial wide-bandgap n-type semiconductor material, is extensively applied in the field of photodetection [7], [8], [9]. It has a relatively wide bandgap, which requires activation by dyes [10], [11]. Graphene, with its unique physical and chemical properties, holds immense value in the development of photodetector devices [12], [13], [14].

Researchers use various methods to enhance the performance of photodetectors. They have designed Schottky heterojunction structures to augment photon absorption and provide stable electron pathways [15]. Sputtering doping coupled with narrow-bandgap semiconductor coupling, sensitization through active dyes, and enhanced light absorption have been explored [16]. Solution composite systems have also been considered as a feasible approach to further enhance their optoelectronic performance [17]. The morphological control of nanomaterials plays a crucial role in their performance, and the performance of optoelectronic devices can be adjusted by reasonably modifying the morphology of nanomaterials [18], such as the modification of nanotube surface scroll-like microstructures and flake-like graphene quantum dots [19], [20]. However, the zero bandgap of

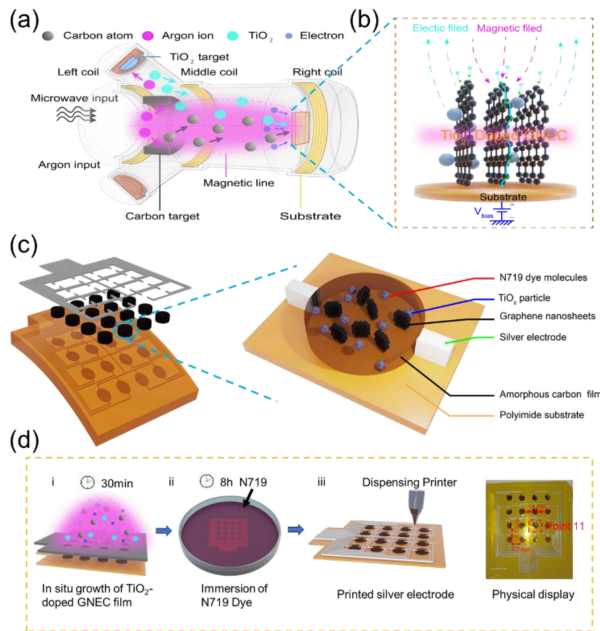


**FIGURE 1.** The fabrication of TiO<sub>2</sub>@GNEC photodetector array. (a) Diagram of ECR system. (b) Diagram illustrating growth of GNs with TiO<sub>2</sub> doping. (c) The structure of a photodetector array. (d) In a single photodetector, TiO<sub>2</sub> particles and GNs are uniformly dispersed within an amorphous carbon film. dye molecules adsorb on the surface of TiO<sub>2</sub> particles. (e) The fabrication process of a photodetector array: (i) In-situ growth of TiO<sub>2</sub>-doped GNEC film spot on a polyimide substrate utilizing a metal mask template, (ii) Immersion in N719 solution for 8 hours, (iii) Printing connection points of the photodetector array using silver paste, physical demonstration of TiO<sub>2</sub>@GNEC photodetector array.

planar graphene results in the lack of an electron capture center [21]. The secondary transfer process of optoelectronic functional materials also brings additional defects.

In this work, we utilized an Electron Cyclotron Resonance (ECR) system to directly manufacture a TiO<sub>2</sub>-doped graphene nanosheets embedded carbon (GNEC) film. The TiO<sub>2</sub>@GNEC photodetector array was fabricated through a simple post-processing method. This ECR system deposits materials in the form of atoms or nanoparticles directly onto flexible substrates, eliminating the need for secondary transfer and ensuring the integrity and strong adhesion of these materials to the substrate. Compared to planar graphene, the vertically aligned Graphene Nanosheets (GNs) in the GNEC film have high-density edges, forming electron-capturing centers. During the process of electron capture and release, GNs suppress the recombination rate with photogenerated holes, significantly extending the lifetime of photogenerated electrons and holes. The TiO<sub>2</sub>@GNEC photodetector exhibits a photo-responsivity of 0.82 mA/W and a response time of 1.93 seconds.

## II. FABRICATION OF FLEXIBLE TiO<sub>2</sub>@GNEC PHOTODETECTOR

Fig. 1a shows the preparation of TiO<sub>2</sub>-doped GNEC film. In the vacuum chamber of the ECR system, the polyimide (purchased from LG Chem) substrate undergoes degreasing treatment with acetone, followed by cleaning with anhydrous

ethanol, and then covered with a mask. The target material for ECR, anatase-phase TiO<sub>2</sub>, was placed in the upper target holder. The chamber was evacuated to  $1 \times 10^{-4}$  Pa and stabilized argon gas was introduced to provide the necessary material for electron cyclotron resonance microwave plasma. Subsequently, the electrical current of the left and middle coil was adjusted to 40A, followed by adjusting the microwave power knob to 500W to excite the electron cyclotron resonance effect. Under the excitation of the argon plasma and the driving of the magnetic field, carbon atoms and TiO<sub>2</sub> nanoparticles were deposited on the substrate, resulting in the vertical growth of TiO<sub>2</sub>-doped GNEC film on the substrate (Fig. 1b). Prior to depositing the film, the substrate surface was cleaned with argon plasma for 3 minutes.

Fig. 1c is a schematic diagram of the final photodetector array and a single photodetector. The detailed fabrication process shown in Fig. 1d. There are several steps: (i) The substrate bias is controlled at +40V to regulate the size of the GNs. The doping current for TiO<sub>2</sub> was controlled at 600 mA to adjust the TiO<sub>2</sub> doping concentration. The deposition time for the film was 30 minutes. The 4×4 TiO<sub>2</sub>-doped GNEC film array is deposited on the polyimide substrate. (ii) 9mg of solid N719 dye powder (purchased from HEPTACHROMA) were placed in a light-protected container, and 25 mL of anhydrous ethanol (purchased from Macklin) was added in. A homogeneous N719 dye solution was obtained by stirring the mixture with a magnetic stirrer in a light-protected environment for 8 hours. The TiO<sub>2</sub>-doped GNEC film in the N719 dye solution was immerse for 8 hours. (iii) The electrodes were drawn out using silver paste (SCD02, purchased from Prtronic).

## III. RESULTS AND DISCUSSION

The morphology of the TiO<sub>2</sub>-doped GNEC film sample were observed under FEI Titan Cubed Themis G2300 aberration-corrected transmission electron microscope (TEM) with an accelerating voltage of 80kV. EDS spectra were acquired using FEI Scios, and Raman spectra were obtained using a laser source with a wavelength of 532 nm from Bruker Senterra-2.

Fig. 2a shows images of the pure carbon film and TiO<sub>2</sub>-doped GNEC film under TEM, with insets showing their fast Fourier transform (FFT) analyses. The red box in the FFT image indicates the presence of two Laue points, corresponding to both sides of a multilayer graphene structure [22], [23]. The blue box shows circular nanoscale shadows with a diameter of approximately 4.54 nm, along with a distinct lattice stripe structure with an interplanar spacing of 0.238 nm. This result aligns with the structure of anatase TiO<sub>2</sub> [24].

Fig. 2b presents the energy dispersive X-ray spectroscopy (EDS) image of TiO<sub>2</sub>-doped GNEC film. Panel i in Fig. 2b illustrates the distribution of carbon elements, panel ii shows the distribution of titanium elements, panel iii indicates the distribution of oxygen elements, and panel iv demonstrates the uniform distribution of carbon, oxygen, and titanium

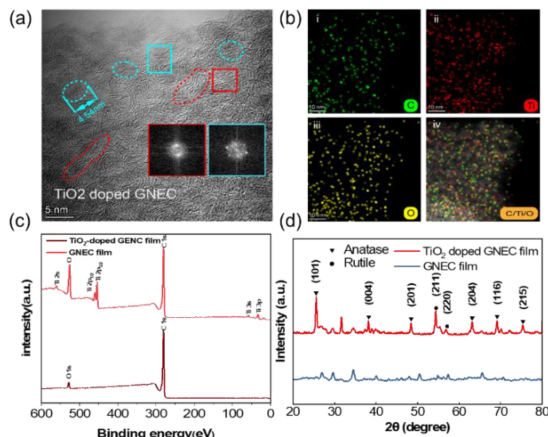


**FIGURE 2.** (a) TEM image of TiO<sub>2</sub>-doped GNEC film: in the FFT image of the region marked in red, two distinct laue spots are observed, indicating the presence of GNs, the blue circle indicates anatase phase TiO<sub>2</sub>. (b) EDS images of TiO<sub>2</sub>-doped GNEC film. (c) XPS full spectrum of the original GNEC film and TiO<sub>2</sub>-doped GNEC film. (d) XRD spectrum of the GNEC film and TiO<sub>2</sub>-doped GNEC film.

elements. The combination of TEM images and EDS images demonstrates that TiO<sub>2</sub> and GNs are dispersed uniformly, achieving atomic and nanoparticulate-level homogeneous doping. Fig. 2c presents the complete X-ray Photoelectron Spectroscopy (XPS) spectra of the GNEC film and TiO<sub>2</sub>-doped GNEC film. The synthesized samples exclusively consist of C, O, and Ti. The binding energies for TiO<sub>2</sub> in the Ti2p3/2, O1s, and C1s peaks are determined to be 458.4 eV, 529.6 eV, and 284.5 eV, respectively. All peak positions in the spectra confirm the presence of TiO<sub>2</sub> and carbon, indicating the absence of any other significant impurities in the samples [25]. In Fig. 2d, X-ray Diffraction (XRD) patterns show diffraction peaks at 25.3°, 37.8°, 48.1°, 62.8°, 68.8°, and 75.1°, corresponding to the anatase phase of TiO<sub>2</sub>, which indicates the presence of anatase TiO<sub>2</sub> in the GNEC film. Additionally, characteristic peaks of rutile TiO<sub>2</sub> are observed at 54.4° and 56.7°, which may result from a partial phase transformation from anatase to rutile during the preparation process. This change is possibly influenced by elevated temperatures.

The possible principle of photoelectric detection for TiO<sub>2</sub>@GNEC photodetector is shown in Fig. 3. In a dark environment, free electrons of GNs migrate in the film in response to an externally applied electric field bias, consequently generating a dark current. The predominant source of these free electrons in this process is GNs. The dark current is diminished due to the capture effect of electrons at the edges of GNs. Upon exposure to light, the dye-TiO<sub>2</sub> particles can release a substantial number of photo-generated electrons. Under the influence of an externally applied electric field bias, these photoelectrons swiftly traverse the GNs network towards the cathode of the external circuit, continuously cycling and forming a photocurrent (Fig. 3a-b). Fig. 3d examines the photo-response of TiO<sub>2</sub>-doped GNEC film compared to pure GNEC film. The photo-response

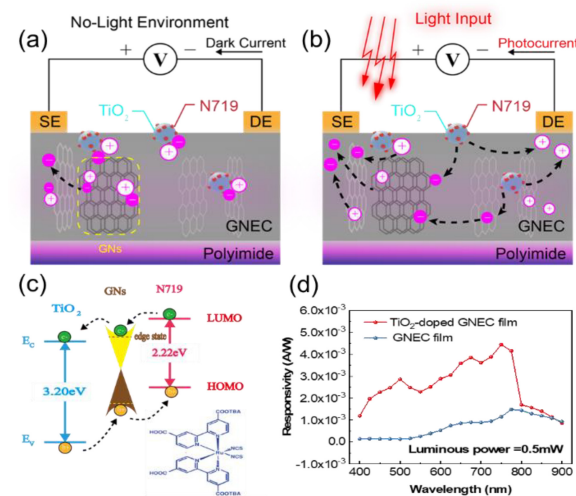


**FIGURE 3.** (a-b) The principle of dark current and photoexcited electrons: dark current primarily originates from the free electrons in GNs. (c) Schematic illustration of energy level diagram for anatase TiO<sub>2</sub>, GNs and N719 dye. (d) The photoelectric response of GNEC film and TiO<sub>2</sub>-doped GNEC film to Light of Different Wavelengths.

rate of the N719-sensitized photodetector is significantly enhanced in the visible light range. The TiO<sub>2</sub>@GNEC photodetector exhibits three distinct peak responses at 500 nm, 675 nm, and 750 nm. When compared to pure GNEC film, the TiO<sub>2</sub>@GNEC photodetector shows a substantial improvement in the maximum response rate, increasing from 1.49 mA/W under 775 nm wavelength illumination to 4.4 mA/W under 750 nm wavelength illumination, a nearly threefold increase.

Under illumination, electrons from the highest occupied molecular orbital (HOMO) of N719 dye are excited to the lowest unoccupied molecular orbital (LUMO) level and injected into the conduction band of TiO<sub>2</sub>. This results in a high absorption intensity of the photodetector in the visible light range of 400nm-780nm, providing a wider range of light detection. The high-density edge states of GNs act as electron-capturing centers, enabling efficient separation of holes and electrons. This allows rapid injection of photoelectrons, and the electrons in the conduction band flow into the external circuit under the influence of an external electric field, generating photocurrent. The oxidized dye molecules accept electrons from the external circuit, regenerating the dye molecules to their reduced state [26], [27]. Consequently, this extends the detection range to include visible light (Fig. 3c). TiO<sub>2</sub> particles characterized by high porosity can absorb a greater quantity of N719 molecules, thereby generating more photoelectrons. Furthermore, the presence of GNs facilitates the rapid transport of photogenerated electrons from N719 to the conduction band of TiO<sub>2</sub>. This process leads to enhanced charge transfer performance and improved light collection efficiency.

As shown in Fig. 4a, under dark conditions, the flexible substrate sample reaches a peak dark current of 19.8nA at

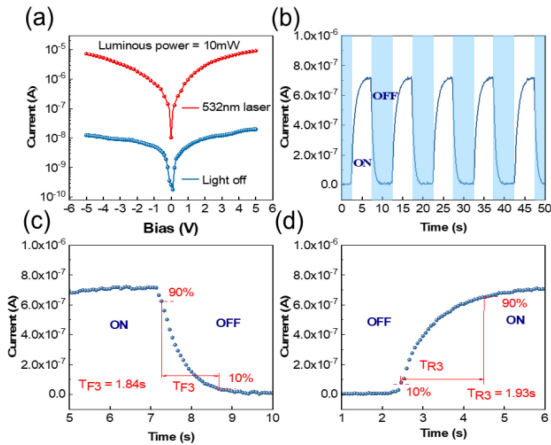


**FIGURE 4.** (a) The dark current and photoelectric current response of  $\text{TiO}_2@\text{GNEC}$  photodetector. (b) Switching cycle curve of  $\text{TiO}_2@\text{GNEC}$  photodetector with a switching interval of 5 seconds. (c-d) The rise and fall time response of  $\text{TiO}_2@\text{GNEC}$  Photodetector.

a  $+5\text{V}$  bias. Under illumination, the maximum photocurrent is  $9.1\mu\text{A}$ . The extremely low dark current is attributed to the capture of some photo-generated electrons at the edges of GNs within GNEC film, this effectively suppresses the recombination of photogenerated electrons with holes [28], [29]. This suppression significantly extends the lifetime of both photo-generated electrons and holes, ultimately resulting in a higher photo-response in  $\text{TiO}_2@\text{GNEC}$  photodetector. The photodetector has a measured rise time ( $T_{F3}$ ) of 1.93 seconds and a fall time ( $T_{R3}$ ) of 1.84 seconds (Fig. 4c-d), with stable response observed over an on-off cycle with a 5-second interval (Fig. 4b).

The bending stability is a crucial metric for evaluating flexibility. The flexible  $\text{TiO}_2@\text{GNEC}$  photodetector was gradually bent from  $0^\circ$  to  $60^\circ$  with a step of  $15^\circ$  using the stretching platform. The quantification of the bending angle followed methodologies reported in the literature [30], [31]. Point 11 was selected as the testing site (Fig. 1d). The responsivity at  $T=0^\circ$  is  $0.82\text{mA/W}$ , while at  $T=60^\circ$ , the responsivity decreases to  $0.31\text{mA/W}$ , representing a 37.8% reduction from the initial responsivity (Fig. 5a). Bending has a negative impact on the photodetector's performance, however, within the tested bending angle range, the flexible  $\text{TiO}_2@\text{GNEC}$  photodetector still maintains a certain level of photodetection capability. The photodetector was repeatedly bent 20 times between  $0^\circ$  and  $60^\circ$ , as shown in Fig. 5b. The maximum photocurrent at  $0^\circ$  decreased from  $8.72\mu\text{A}$  to  $7.91\mu\text{A}$ , by 9.3% reduction. While at  $60^\circ$ , the maximum photocurrent decreased from  $3.32\mu\text{A}$  to  $2.98\mu\text{A}$ , a 10.2% reduction. The photodetection response of all 16 points was individually tested, and the dark current across all test points ranged from  $2.12\text{nA}$  to  $9.35\text{nA}$  (Fig. 5c). From Fig. 5d, it is evident that the photocurrent generated by each point under illuminations of  $0.1\text{mA}$ ,  $1\text{mA}$ , and  $10\text{mA}$  is distributed within a relatively narrow range, demonstrating the excellent uniformity of the flexible  $\text{TiO}_2@\text{GNEC}$  photodetector. The

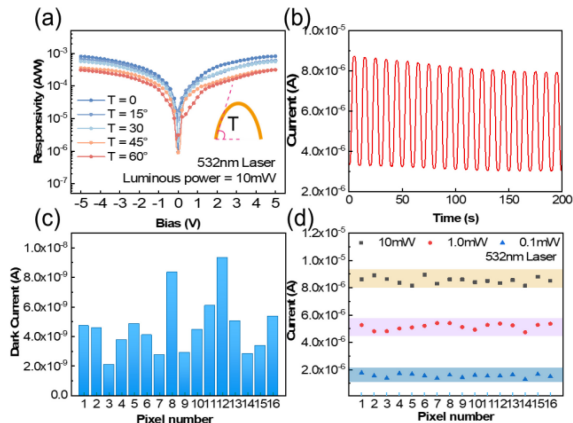


**FIGURE 5.** (a) Photoresponsivity at  $0^\circ$  -  $60^\circ$ . (b) Cycle performance testing. (c) Dark current testing of 16 points. (d) The photocurrent distribution of 16 points at  $0.1\text{mW}$ ,  $1\text{mW}$ , and  $10\text{mW}$  illumination.

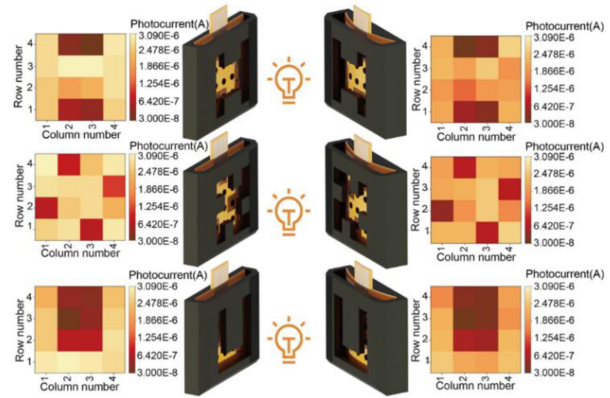


**FIGURE 6.** Visual imaging testing.

consistency is credited to the ECR system's in-situ manufacturing capabilities, which decrease defects during device fabrication.

We tested the visual imaging capability of the  $\text{TiO}_2@\text{GNEC}$  photodetector array. The photodetector array was placed inside a black box with various shadow patterns. The bottom of the black box on the left was flat, while the one on the right had a curved surface with a radius of curvature of 80mm. The  $\text{TiO}_2$ -doped GNEC film remains firmly attached to the polyimide substrate even under bending conditions. White light from a spotlight was directed onto the photodetector array through the shadow patterns. In this configuration, the points exposed to light exhibited higher photo-response, while the shaded points showed lower photo-response. The thermal map of the photodetector array accurately reproduced the shape of the mask.

Fig. 6 on the left demonstrates the imaging results in the unbent state, while the right side shows the imaging results in the bent state. In the bent state, the photocurrent values at various points decrease when exposed to light, consistent with the decrease in the photodetection capability of individual points when bent. The thermal map of the

photodetector array accurately reproduced the shape of the mask.

#### IV. CONCLUSION

In summary, we utilized ECR technology to in-situ grow TiO<sub>2</sub>-doped GNEC film array on polyimide substrates. TiO<sub>2</sub>@GNEC photodetector array were fabricated by dye sensitization and printing external circuits. N719 dye sensitization broadened the photo-response range, while the edge states of GNs effectively separated photo-generated electrons and holes, enhancing the photo-response rate. The photodetector exhibited a wide response wavelength range of 400nm–780nm, a photo-response rate of 0.82 mA/W, and a response time of 1.93 seconds, which is three times that of GNEC film. Thanks to the in-situ manufacturing advantages of ECR, the 16-detector array points demonstrated excellent consistency and were able to accurately recognize patterned light sources even in a bent state. This study provides an effective method for the direct fabrication of high-performance photodetectors on flexible substrates.

#### REFERENCES

- [1] Z. Chen et al., "Ultrasensitive DNA origami plasmon sensor for accurate detection in circulating tumor DNAs," *Laser Photonics Rev.*, May 2024, Art. no. 2400035, doi: [10.1002/lpor.202400035](https://doi.org/10.1002/lpor.202400035).
- [2] Y. Xu and Q. Lin, "Photodetectors based on solution-processable semiconductors: Recent advances and perspectives," *Appl. Phys. Rev.*, vol. 7, no. 1, Mar. 2020, Art. no. 011315, doi: [10.1063/1.5144840](https://doi.org/10.1063/1.5144840).
- [3] Y. Zhao, C. Li, J. Jiang, B. Wang, and L. Shen, "Sensitive and stable tin-lead hybrid perovskite photodetectors enabled by double-sided surface passivation for infrared upconversion detection," *Small*, vol. 16, no. 26, Jul. 2020, Art. no. 2001534, doi: [10.1002/smll.202001534](https://doi.org/10.1002/smll.202001534).
- [4] W. Huang et al., "Enhanced Photodetection properties of tellurium@selenium roll-to-roll nanotube heterojunctions," *Small*, vol. 15, no. 23, Jun. 2019, Art. no. 1900902, doi: [10.1002/smll.201900902](https://doi.org/10.1002/smll.201900902).
- [5] Y. Liu, M. Pharr, and G. A. Salvatore, "Lab-on-skin: A review of flexible and stretchable electronics for wearable health monitoring," *Acs Nano*, vol. 11, no. 10, pp. 9614–9635, Oct. 2017, doi: [10.1021/acsnano.7b04898](https://doi.org/10.1021/acsnano.7b04898).
- [6] H.-H. Zuo et al., "Ultra-sensitive narrow-band P-Si Schottky photodetector with good wavelength selectivity and low driving voltage," *IEEE Electron Device Lett.*, vol. 45, no. 1, pp. 68–71, Jan. 2024, doi: [10.1109/led.2023.3331048](https://doi.org/10.1109/led.2023.3331048).
- [7] H. Algadi, H. Albargi, A. Umar, and M. Shkir, "Enhanced photoresponsivity of anatase titanium dioxide (TiO<sub>2</sub>)/nitrogen-doped graphene quantum dots (N-QDs) heterojunction-based photodetector," *Adv. Composites Hybrid Mater.*, vol. 4, no. 4, pp. 1354–1366, Dec. 2021, doi: [10.1007/s42114-021-00355-5](https://doi.org/10.1007/s42114-021-00355-5).
- [8] M. B. Sarkar et al., "Improved UV photodetection by Indium Doped TiO<sub>2</sub> Thin Film Based photodetector," *J. Nanosci. Nanotechnol.*, vol. 18, no. 7, pp. 4898–4903, Jul. 2018, doi: [10.1166/jnn.2018.15295](https://doi.org/10.1166/jnn.2018.15295).
- [9] J. Zhang, F. Feng, T. Wang, and X. Yuan, "Bulk recrystallization for high-responsivity and stable formamidinium-based quasi-2D perovskite photodetector," *IEEE Electron Device Lett.*, vol. 45, no. 1, pp. 80–83, Jan. 2024, doi: [10.1109/led.2023.3335850](https://doi.org/10.1109/led.2023.3335850).
- [10] B. Yu, L. Zhang, and G. Zhang, "Preparation and photocatalytic performance of C/N Co-doped rich-defect tio2 by dielectric barrier discharge plasma," *J. Mol. Struct.*, vol. 1284, Jul. 2023, Art. no. 135366, doi: [10.1016/j.molstruc.2023.135366](https://doi.org/10.1016/j.molstruc.2023.135366).
- [11] A. Meng, L. Zhang, B. Cheng, and J. Yu, "Dual cocatalysts in TiO<sub>2</sub> photocatalysis," *Adv. Mater.*, vol. 31, no. 30, Jul. 2019, Art. no. 1807660, doi: [10.1002/adma.201807660](https://doi.org/10.1002/adma.201807660).
- [12] A. Tomadin et al., "The ultrafast dynamics and conductivity of photoexcited graphene at different Fermi energies," *Sci. Adv.*, vol. 4, no. 5, May 2018, Art. no. eaar5313, doi: [10.1126/sciadv.aar5313](https://doi.org/10.1126/sciadv.aar5313).
- [13] S. Zhang et al., "High-performance near-infrared photodetector by integration of PbS quantum dots with 3D-graphene," *IEEE Electron Device Lett.*, vol. 44, no. 8, pp. 1240–1243, Aug. 2023, doi: [10.1109/led.2023.3288140](https://doi.org/10.1109/led.2023.3288140).
- [14] Z. Chen et al., "A CRISPR/Cas12a-empowered surface plasmon resonance platform for rapid and specific diagnosis of the Omicron variant of SARS-CoV-2," *Nat. Sci. Rev.*, vol. 9, no. 8, Aug. 2022, Art. no. nwac104, doi: [10.1093/nsr/nwac104](https://doi.org/10.1093/nsr/nwac104).
- [15] H. Algadi, J. N. Ren, and A. Alqarni, "A high-performance self-powered photodetector based on solution-processed nitrogen-doped graphene quantum dots/all-inorganic perovskite heterostructures," *Adv. Compos. Hybrid Mater.*, vol. 6, no. 3, p. 98, Jun. 2023, doi: [10.1007/s42114-023-00688-3](https://doi.org/10.1007/s42114-023-00688-3).
- [16] S. Majumder, D. Paramanik, V. Solanki, B. Bag, and S. Varma, "Bandgap tailoring of rutile TiO<sub>2</sub>(110) via surface patterning with electron cyclotron resonance sputtering," *Appl. Phys. Lett.*, vol. 98, no. 5, Jan. 2011, Art. no. 053105, doi: [10.1063/1.3549768](https://doi.org/10.1063/1.3549768).
- [17] D. Xiong et al., "Controllable *in-situ*-oxidization of 3D-networked Ti<sub>3</sub>C<sub>2</sub>T<sub>x</sub>-TiO<sub>2</sub> photodetectors for large-area flexible optical imaging," *Nano Energy*, vol. 93, Mar. 2022, Art. no. 106889, doi: [10.1016/j.nanoen.2021.106889](https://doi.org/10.1016/j.nanoen.2021.106889).
- [18] W. Huang et al., "Emerging mono-elemental bismuth nanostructures: Controlled synthesis and their versatile applications," *Adv. Funct. Mater.*, vol. 31, no. 10, Mar. 2021, Art. no. 2007584, doi: [10.1002/adfm.202007584](https://doi.org/10.1002/adfm.202007584).
- [19] T. Xue et al., "Ultrasensitive detection of miRNA with an antimonene-based surface plasmon resonance sensor," *Nat. Commun.*, vol. 10, p. 28, Jan. 2019, doi: [10.1038/s41467-018-07947-8](https://doi.org/10.1038/s41467-018-07947-8).
- [20] W. Huang, M. Wang, L. Hu, C. Wang, Z. Xie, and H. Zhang, "Recent advances in semiconducting monoelemental selenium nanostructures for device applications," *Adv. Funct. Mater.*, vol. 30, no. 42, Oct. 2020, Art. no. 2003301, doi: [10.1002/adfm.202003301](https://doi.org/10.1002/adfm.202003301).
- [21] T. K. Agarwal et al., "Bilayer graphene tunneling FET for sub-0.2 V digital CMOS logic applications," *IEEE Electron Device Lett.*, vol. 35, no. 12, pp. 1308–1310, Dec. 2014, doi: [10.1109/led.2014.2364260](https://doi.org/10.1109/led.2014.2364260).
- [22] S. Nosheen, F. S. Galasso, and S. L. Suib, "Role of Ti-O bonds in phase transitions of TiO<sub>2</sub>," *Langmuir*, vol. 25, no. 13, pp. 7623–7630, Jul. 2009, doi: [10.1021/la9002719](https://doi.org/10.1021/la9002719).
- [23] M. H. Tran, J.-S. Bae, and J. Hur, "Self-powered, transparent, flexible, and solar-blind deep-UV detector based on surface-modified TiO<sub>2</sub> nanoparticles," *Appl. Surface Sci.*, vol. 604, Dec. 2022, Art. no. 154528, doi: [10.1016/j.apsusc.2022.154528](https://doi.org/10.1016/j.apsusc.2022.154528).
- [24] E. Cako et al., "Heterojunction of (P, S) co-doped g-C3N4 and 2D TiO<sub>2</sub> for improved carbamazepine and acetaminophen photocatalytic degradation," *Sep. Purif. Technol.*, vol. 311, Apr. 2023, Art. no. 123320, doi: [10.1016/j.seppur.2023.123320](https://doi.org/10.1016/j.seppur.2023.123320).
- [25] L. Wang et al., "Long-range ordered carbon clusters: A crystalline material with amorphous building blocks," *Science*, vol. 337, no. 6096, pp. 825–828, Aug. 2012, doi: [10.1126/science.1220522](https://doi.org/10.1126/science.1220522).
- [26] P. Parreira et al., "Dye-sensitized 1D anatase TiO<sub>2</sub> nanorods for tunable efficient photodetection in the visible range," *Sens. Actuators B-Chem.*, vol. 161, no. 1, pp. 901–907, Jan. 2012, doi: [10.1016/j.snb.2011.11.059](https://doi.org/10.1016/j.snb.2011.11.059).
- [27] F. Jahantigh, S. M. B. Ghorashi, and A. Bayat, "Hybrid dye sensitized solar cell based on single layer graphene quantum dots," *Dyes Pigments*, vol. 175, Apr. 2020, Art. no. 108118, doi: [10.1016/j.dyepig.2019.108118](https://doi.org/10.1016/j.dyepig.2019.108118).
- [28] X. Zhang, L. Tian, and D. Diao, "High-response heterojunction phototransistor based on vertically grown graphene nanosheets film," *Carbon*, vol. 172, pp. 720–728, Feb. 2021, doi: [10.1016/j.carbon.2020.10.054](https://doi.org/10.1016/j.carbon.2020.10.054).
- [29] Z. Lin, Z. Wang, X. Zhang, and D. Diao, "Superhydrophobic, photo-sterilize, and reusable mask based on graphene nanosheet-embedded carbon (GNEC) film," *Nano Res.*, vol. 14, no. 4, pp. 1110–1115, Apr. 2021, doi: [10.1007/s12274-020-3158-1](https://doi.org/10.1007/s12274-020-3158-1).
- [30] G. Zhou, R. Sun, Y. Xiao, G. Abbas, and Z. Peng, "A high-performance flexible broadband photodetector based on graphene-PTAA-perovskite heterojunctions," *Adv. Electron. Mater.*, vol. 7, no. 3, Mar. 2021, Art. no. 2000522, doi: [10.1002/aem.202000522](https://doi.org/10.1002/aem.202000522).
- [31] S. Cai, X. Xu, W. Yang, J. Chen, and X. Fang, "Materials and designs for wearable photodetectors," *Adv. Mater.*, vol. 31, no. 18, May 2019, Art. no. 1808138, doi: [10.1002/adma.201808138](https://doi.org/10.1002/adma.201808138).